SCANNING TUNNELLING MICROSCOPY AND ELECTROCHEMICAL RESPONSE OF ELECTROFACETTED GOLD ELECTRODES

J. GÓMEZ, L. VÁSQUEZ and A. M. BARÓ

Departamento de Física de Materia Condensada, C-III, Facultad de Ciencias, Universidad Autónoma de Madrid, Cantoblanco, 28049, Madrid, España

C. L. PERDRIEL and A. J. ARVIA

Instituto de Investigaciones Fisicoquimicas Teóricas y Aplicadas (INIFTA), Facultad de Ciencias Exactas, Universidad Nacional de La Plata, Sucursal 4, Casilla de Correo 16, (1900) La Plata, Argentina

Abstract—A first attempt to establish a direct correlation between *ex situ* scanning tunnelling microscopy imaging and voltammetric features of gold electrodes is presented. For this purpose gold microelectrodes, either polyfacetted or electrochemically facetted were used. The STM topography of polyfacetted gold microelectrodes exhibits flat domains and regions with a number of different defects, whereas that of electrofacetted gold presents a parallel ridge-like structure of a few atoms height together with other types of defects. Lead UPD and voltammetric stripping reactions for the O-electroadsorption–electrodesorption reactions both in acid solution were selected as test reactions. The correlation between STM topography and voltammetry data supports qualitatively the assignments made for lead UPD peaks resulting on different gold single crystal surfaces.

INTRODUCTION

Scanning Tunnelling Microscopy (STM)[1, 2] has recently been used as an *ex situ* technique to investigate the topography at the nm level of various types of electrodes, such as electrochemically facetted platinum electrodes[3, 4], large active area platinum and gold electrodes[5, 6] and some amorphous metal alloys of possible application in water electrolysis[7]. This communication is devoted to discover the changes in topography at the nanometer level of bead gold electrodes made by employing the fusion–solidification technique[8] which have been subjected to electrochemical facetting treatment [9, 10], and to relate the topography changes to the modifications of the electrochemical spectrum for the underpotential deposition (UPD) of lead on the different electrofacetted gold electrode surfaces. The influence of the crystallographic faces of gold on the lead UPD reaction has been extensively investigated at well-defined single crystal gold electrodes[11, 12]. These results were taken as electrochemical references in the present work.

EXPERIMENTAL

The experimental work comprises three different parts, namely, the electrode preparation and treatment, the determination of the surface topography through STM imaging, and the Pb UPD on the different gold electrodes.

Electrode preparation

Spherical shaped gold working electrodes were prepared from a polycrystalline gold wire (0.5 mm dia. Engelhard, specpure gold) by melting one extremity of the wire in an air–gas torch flame and quenching in air. The electrode geometrical area resulting for the gold spheres ranged between 0.03 and 0.07 cm². The gold electrodes which result from the preparation procedure just described are denoted as Electrode I.

Electrochemical facetting

Gold electrodes (Electrode I) were subjected to electrochemical facetting treatment at 25°C in 4 M HF, by applying a repetitive square wave potential scanning between the following potential limits, E_l = 0.50 and E_u = 1.70 V, at the frequency f = 2.5 kHz during t_1 = 2 h (Electrode II). These are the optimal conditions for obtaining a gold preferred oriented surface in the (210) direction[13]. The same procedure was also applied for 7.5 h (Electrode III). The 4 M HF solution was prepared from Carlo Erba RPE 40% HF and Millipore water. The experimental set-up employed in the electrochemical facetting treatment consisted of a cell arrangement which assured the best current distribution compatible with the simplest cell design. A M-5 Lyp potentiostat coupled to a Lyp square wave generator was used. The characteristics of the potentiostat were: output current ± 1 A; resolution ± 1 mV; scan rate 2 V μs^{-1}; accuracy 0.2%; linearity 0.25%; ohmic drop compensation up to 100 kΩ and rise time

5 μs. Potentials are referred to the reversible hydrogen electrode in the same solution (rhe).

STM imaging

Ex situ STM images of Electrodes I, II and III were obtained in air. The microscope used was of the so-called pocket size type[14] which uses a stack of metal plates separated by viton spacers to absorb external mechanical vibrations. Data were taken at several tunnelling voltages (tip positive) and a tunnelling current of 10 μA. The scanning frequency was placed at 0.1 Hz.

The images were obtained by plotting the voltage applied to the tip piezodrives on a x–y recorder. At the same time the data were acquired with a DACA card installed on a IBM PC-AT and stored on a hard disc in order to be processed subsequently. Data processing consisted of the following steps: (i) treatment of the data with a smoothing filter; (ii) removal of a background plane to eliminate the lack of perpendicularity between the sample and the tip; (iii) image processing. The processed images were displayed essentially in two different ways, namely, a three-dimensional display taken with any orientation, in particular 90° (top view), and illuminated laterally, and a contour map of equal corrugation lines or its equivalent using colour or gray scale. The images could be rotated around the z-axis by any angle in order to make apparent hidden features.

Underpotential deposition of lead

The electrochemical behaviour of the different gold electrodes was firstly followed through conventional voltammetry in 4 M HF at 0.1 V s^{-1} in the 0.4–1.7 V range. However, as for gold electrodes the O-electroadsorption–electrodesorption spectrum is less sensitive to changes in the crystallographic face distribution of gold than Pb upd and stripping voltammogram, the latter reaction was preferred as a reference to attempt a comparison to the surface topography of gold electrodes. For this purpose, the voltammograms of UPD Pb on gold at 0.02 V s^{-1} were also run in 1 M HClO$_4$ + 1 × 10^{-3} M Pb(ClO$_4$)$_2$. These voltammograms can be directly compared to those already reported in the literature[11, 12]. The potential values for Pb UPD voltammetry are referred to a rhe in 1 M HClO$_4$. All voltammetric runs were made at 25° C by using conventional circuitry.

RESULTS

Voltammetric data

The voltammogram run with Electrode I (blank) (Fig. 1, dashed trace) in 4 M HF exhibits a complex anodic profile between ca 1.35 and ca 1.70 V with a relatively sharp anodic current peak at 1.38 V which overlaps to a great extent the second wide anodic current peak located in the 1.4–1.7 V range. The voltammetric anodic charge density, Q_a^0, is related to the electroformation of O-containing surface species. The returning cathodic scan presents a sharp current peak at about 1.15 V with an additional contribution at its descending current branch both related to the
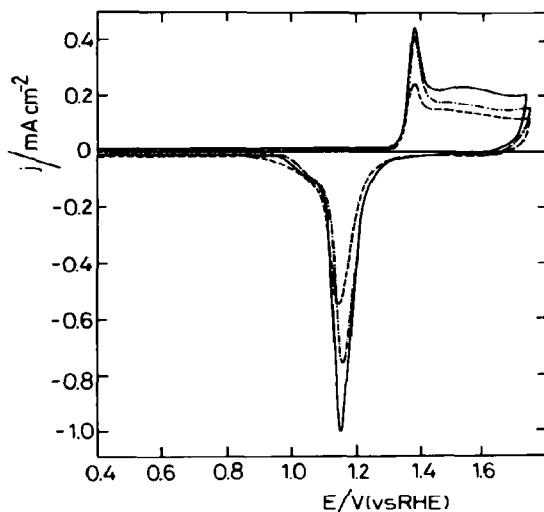

Fig. 1. Voltammograms run in 4 M HF at 0.10 V s^{-1} and 25° C. (– – –) bead-shaped Au electrode (Electrode I); (– · –) bead-shaped Au electrode after 2 h RSWPS in 4 M HF at f = 2.5 kHz, between E_1 = 0.50 and E_s = 1.70 V (Electrode II); (——) bead-shaped Au electrode after 7 h RSWPS in 4 M HF at f = 2.5 kHz, between E_1 = 0.50 and E_u = 1.70 V (Electrode III).

electroreduction of the O-containing surface layer, the corresponding charge density being Q_c^0. The equality $Q_a^0/Q_c^0 = 1 \pm 0.02$ beholds for all voltammograms. The voltammetric responses under comparable conditions of Electrodes II and III (Fig. 1, full and dashed-point traces) show a substantial increase in the height of the anodic current peaks located at 1.4 and 1.15 V, and correspondingly, an increase in the entire voltammetric charge with respect to that obtained for electrode I. The increase in the ratio of voltammetric charge density expressed as $(Q_c^0)_i/(Q_c^0)_I$, where i = II and III, is 1.2 for Electrode II and 1.6 for Electrode III. This change in $(Q_c^0)_i/(Q_c^0)_I$ ratio can be due to a relative change in the contribution of crystallographic faces or
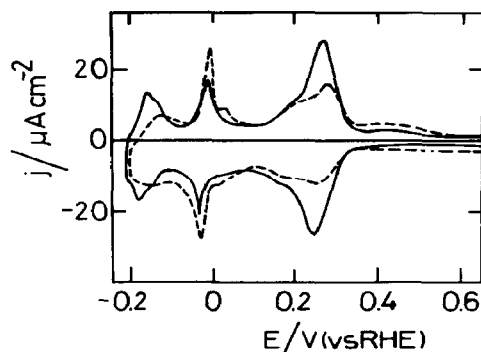

Fig. 2. Voltammograms run in 1 M HClO$_4$ + 1 × 10^{-3} M Pb(ClO$_4$)$_2$ at 0.020 V s^{-1}. (– – –) bead-shaped Au electrode; (——) bead-shaped Au electrode after 3 h RSWPS in 4 M HF at f = 2.5 kHz between E_1 = 0.50 V and E_u = 1.70 V.

defects provided that each current peak actually reflects the O-electrodesorption reaction at a particular crystallographic face or defect.

The UPD voltammogram for lead on polyfacetted gold (Fig. 2) exhibits three pairs of reversible conjugate current peaks at about −0.18 V, at −0.02 V and 0.26 V, respectively. According to the literature each pair of peaks is related to the reaction undergoing at a particular type of surface sites. Thus, the first pair of peaks was assigned to the reaction at steps containing only a few atoms, the second one to (111)-terraces

and the third one to stepped (110) faces[11, 12]. On the other hand, the charge distribution for the UPD Pb voltammetric peaks is substantially modified for the facetted gold electrodes as compared to electrode I. For electrofacetted gold a net predominance of the pair of peaks at 0.26 V can be noticed.

Ex situ *STM imaging*

The *ex situ* STM topography of Electrode I (untreated) at different scales (Fig. 3) exhibits a large

(a)

(b)

(c)

(d)

(e)
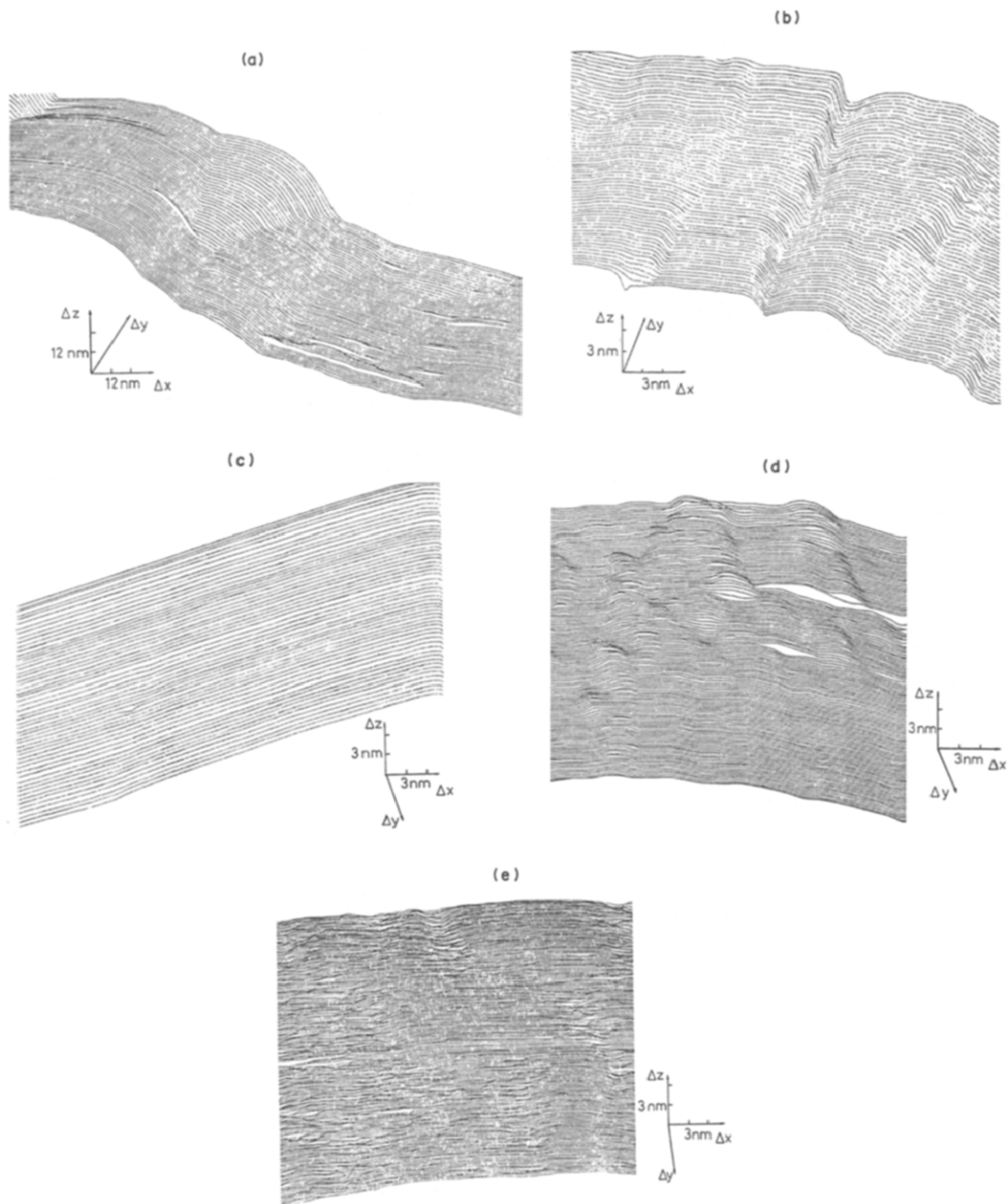
number of non-uniformly distributed defects (Fig. 3a) large rounded steps which define relatively smooth surface terraces, containing only a small number of irregular steps. The different types of defects can be better described through images at 3×3 nm scale (Fig. 3b). In this case one can distinguish clear steps of about 3 nm height, very flat surface regions (Fig. 3c), randomly distributed dome-like (Fig. 3d) and spike-like (Fig. 3e) structures. Similar structures were also found at platinum electrodes surfaces with different crystallographic orientations[3, 4].

The topography of Electrode II (treated) at the 12 $\times$ 12 nm scale (Fig. 4a) exhibits domains determined by steps which are oriented in two defined directions cut at ca 90°. These domains can be as large as about 100×100 nm (Fig. 4a) or much smaller. The small domains exhibit a surface topography at the 12 $\times$ 12 nm level constituted by a set of nearly flat terraces of about 10^2 nm. Each domain also contains a nearly periodic wavy structure resulting in parallel channels of only 3 nm in height (Fig. 4b), approximately. The same type of topography can be described for Electrode III (treated). The preferred oriented channel-like structure involves defective steps as seen from a three dimensional view resulting from both Electrode II and III. According to the pictures depicted in Fig. 5a for Electrode III, the average width of each

ridge is about 15 nm and its average height is about 2 nm. However, after a prolonged electrochemical facetting (Figs 5b and c) very flat domains with steps of atomic height can be also produced as it occurred for electrochemical facetted platinum[3].

DISCUSSION

STM imaging shows that a polyfacetted gold microsphere involves a complex surface topography with different types of defects. There are relatively large domains which can be considered atomically flat, together with regions which exhibit relatively large steps with heights in the range of a few atoms diameter. Likewise, the distribution of defects changes smoothly over the surface.

Otherwise, the STM images of electrofacetted gold electrodes show surface regions with a clear crystallographic orientation characterized by a corrugation at certain surface domains (Figs 4a and 5b) which is comparable to that previously reported for gold (100) single crystals[15] and for reconstructed gold (110) surfaces[16]. Nevertheless, the electrochemical facetted gold surface is somewhat more complex than that of platinum hitherto reported[3, 4]. In the case of gold the corrugated ridge-like structures are related to the formation of a relatively wide (about 50 atoms dia.) low height (about 3–5 atoms dia.) steps. These stepped surfaces consisting apparently of a few terraces separated by one atom high step originate a relatively great surface concentration of higher index crystal faces. This means that a section of each ridge can be imagined as builtup by piling up about five layers of metal atoms starting from one with about 50 atoms at the front side and following with other layers with a decreasing number of atoms. The possible combination of rows with different number of atoms originates many defects at the atomic scale on each ridge-like structure. In addition, this complex atomic arrangement should also involve the formation of kinks. Therefore, through the electrochemical facetting treatment one can conclude that the gold surface becomes stable in a sort of a monoatomic step configuration, which is generally the case described for clean metal surfaces[17].

The conclusions about gold electrode topography derived from STM can be related to voltammetric data (Figs 1 and 2), either for O-electroadsorption or UPD lead on the electrofacetted gold electrodes. For this purpose the assignment of voltammetric peaks made in the literature[11, 12] for gold single crystal faces has been taken as reference. This relation can be much more clearly illustrated through the voltammograms for UPD lead. For electrofacetted gold the voltammetric peak at -0.02 V which was assigned to the desorption of lead from (111) terraces decreases significantly. It is interesting to notice that the voltammogram shown in Fig. 6 resembles closely that obtained by combining the voltammograms of (210) and (211) crystal faces (Fig. 6c). These surfaces can be builtup from a combination of different faces such as the following ones:

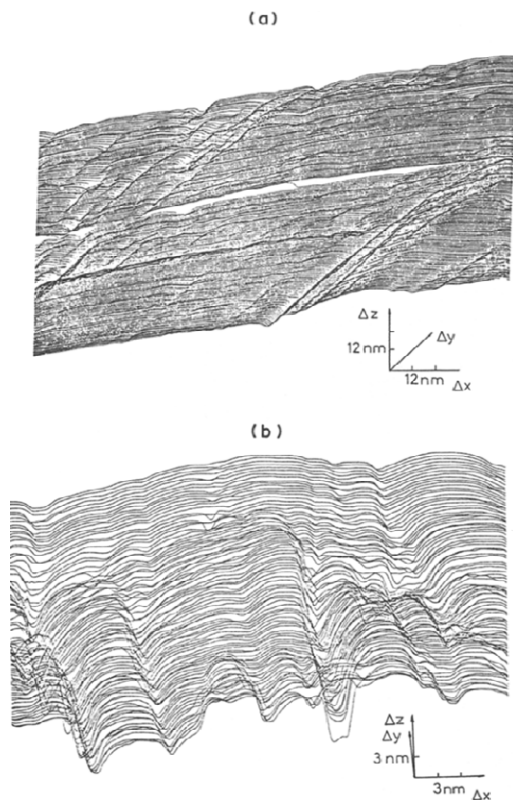$$(210) = 2(110) \times (100),$$

$$(211) = 3(111) \times (100),$$

(a)

(b)

Fig. 4. STM images of a bead-shaped Au treated electrode (Electrode II). The topographic features are described in the text.
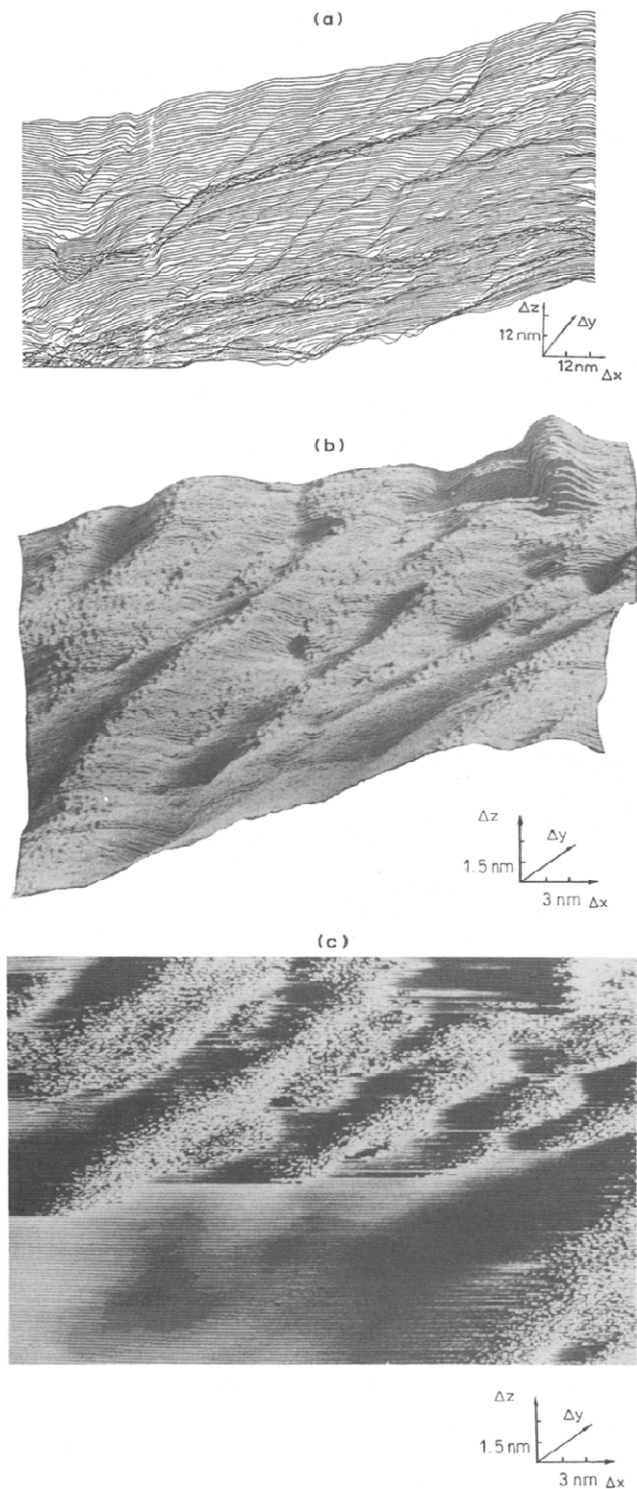
(a)

(b)

(c)

Fig. 5. STM images of a bead-shaped Au treated electrode (Electrode III): (a) image obtained with an $x-y$ recorder; (b) STM 3-D processed imaged illuminated laterally; (c) same as (b) but seen from the top. The processed images make clearer the orientation of ridges.
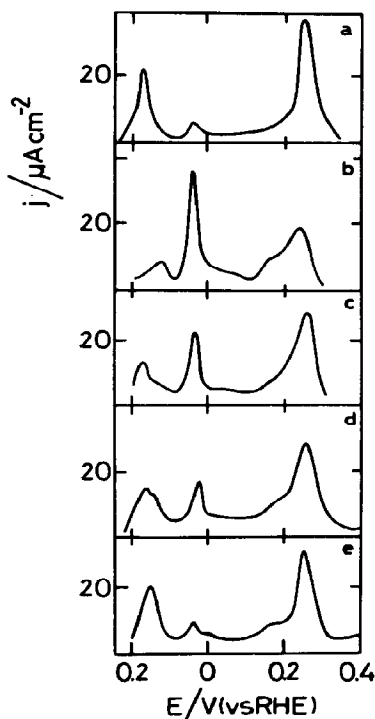
Fig. 6. Voltammograms run at $0.020 \, V s^{-1}$: (a) gold (210) $1 \times 10^{-3} \, M \, PbF_2 + 1 \times 10^{-3} \, M \, HClO_4$[12]; (b) gold (211) 1 $\times 10^{-3} \, M \, PbF_2 + 1 \times 10^{-3} \, M \, HClO_4$[12]; (c) addition of gold (210) (50%) and gold (211) (50%), $1 \times 10^{-3} \, M \, PbF_2 + 1 \times 10^{-3} \, M \, HClO_4$[12]; (d) electrofaceted gold electrode in 4 M HF at 2.5 kHz, $E_u = 1.70 \, V$, $E_1 = 0.50 \, V$, $t = 3 \, h$; 1 $\times 10^{-3} \, M \, Pb(ClO_4)_2 + 1 \, M \, HClO_4$; (e) electrofaceted gold electrode at 2.5 kHz, $E_u = 1.70 \, V$, $E_1 = 0.50 \, V$, $t = 9 \, h$; $1 \times 10^{-3} \, M \, Pb(ClO_4)_2 + 1 \, M \, HClO_4$.

which correspond to a structure of steps and terraces. Likewise, when the electrochemical facetting treatment at $f = 2.5 \, kHz$, $E_1 = 0.05 \, V$ and $E_u = 1.70 \, V$ is run for $t = 9 \, h$, the voltammogram of the treated gold electrode exhibits still a further decrease of the peak at $-0.02 \, V$. Then, the resulting voltammogram becomes nearly identical to that reported for gold (210) single crystal electrode. It should also be noticed that the (210) crystallographic face of gold exhibits the lowest potential of zero charge $(E_z[(210)Au] = 0.13 \, V$ vs sce correspondingly the greatest work function value and according to the TLK model, the greatest roughness[18]. Furthermore, there is no specific adsorption of $NaBF_4$ in solution on the (210) Au face, at least in the neighbourhood of E_z, as it occurs for the (111) Au face[19]. Otherwise, the electrochemical properties of the gold (211) crystal faces are closely similar to those already mentioned for the (210) faces[18–20]. The same conclusions can be derived from the voltammograms for UPD lead stripping.

On the other hand, for the electrofacetted gold electrodes, the voltammograms shown in Figs 1 and 2 (solid lines) involve a predominant contribution of anodic current peaks at about 1.4 V for O-electroadsorption and about 0.26 and $-0.18 \, V$ for the stripping of UPD lead. These peaks are assigned to the electrochemical reactions undergoing at steps[11, 12]. Hence, this voltammetric behaviour also correlates reasonably well with the STM imaging of gold electrode surface at the atomic level.

In conclusion, the voltammetric features of gold electrode surfaces either polyfacetted or electrochemically facetted can be directly correlated to the electrode surface topography throughout the different domains of crystallographic order of surface particles as resulting from *ex situ* STM imaging.

REFERENCES

1. G. Binnig and H. Rohrer, *Helv. Phys. Lett.* **55**, 726 (1982).
2. G. Binnig and H. Rohrer, *Surf. Sci.* **126**, 236 (1983).
3. J. Gómez, L. Vázquez, A. M. Baró, N. García, C. L. Perdriel, W. E. Triaca and A. J. Arvia, *Nature* **323**, 612 (1986).
4. L. Vázquez, J. M. Gómez Rodríguez, J. Gómez Herrero, A. M. Baró, N. García, J. C. Canullo and A. J. Arvia, *Surf. Sci.* **181**, 98 (1987).
5. L. Vázquez, J. Gómez, A. M. Baró, N. García, M. L. Marcos, J. González Velasco, J. M. Vara, A. J. Arvia, J. Presa, A. García and M. Aguilar, *J. Am. chem. Soc.* **109**, 1730 (1987).
6. J. Gómez, L. Vázquez, A. M. Baró, C. Alonso, E. González, J. González-Velasco and A. J. Arvia, *J. electroanal. Chem.* **240**, 77 (1988).
7. G. Kreysa, J. Gomez, A. M. Baró and A. J. Arvia, submitted.
8. J. Clavilier, *J. electroanal. Chem.* **107**, 211 (1980).
9. A. J. Arvia, J. C. Canullo, E. Custidiano, C. L. Perdriel and W. E. Triaca, *Electrochim. Acta* **31**, 612 (1986).
10. C. L. Perdriel, M. Ipohorsky and A. J. Arvia, *J. electroanal. Chem.* **215**, 317 (1986).
11. A. Hamelin, *J. electroanal. Chem.* **165**, 167 (1984).
12. A. Hamelin and L. Lipkowski, *J. electroanal. Chem.* **171**, 317 (1984).
13. M. C. Galindo, C. L. Perdriel, M. E. Martins and A. J. Arvia, *Langmuir*, in press.
14. M. Anders, M. Thaer and C. Heiden, *Surf. Sci.* **181**, 176 (1987). J. G. H. Hermsen, H. van Kempen, B. J. Nelissen, L. L. Soethout, G. F. A. van de Walle, P. J. W. Weijs and P. Wyder, *Surf. Sci.* **181**, 183 (1987).
15. R. Miranda, N. García, A. M. Baró, R. García, J. L. Peña and H. Rohrer, *Appl. Phys. Lett.* **47**, 367 (1985).
16. G. Binnig, H. Rohrer, Ch. Gerber and E. Weibel, *Surf. Sci.* **134**, 379 (1983).
17. D. G. Castuer and G. A. Somorjai, *Chem. Rev.* **79**, 233 (1979).
18. J. Lecoeur, J. Andro and R. Parsons, *Surf. Sci.* **114**, 320 (1982).
19. A. Hamelin, Z. Borkowska and J. Stafiej, *J. electroanal. Chem.* **189**, 85 (1985).
20. A. Hamelin, T. Vitanov, E. Sevastyanov and A. Popov, *J. electroanal. Chem.* **145**, 225 (1983).